IET Electric Power Applications

Research Article

IET Journals
The Institution of Engineering and Technology

Space-vector state dynamic model of *SynRM* considering self- and cross-saturation and related parameter identification

ISSN 1751-8660
Received on 19th June 2020
Revised 9th November 2020
Accepted on 15th December 2020
E-First on 2nd March 2021
doi: 10.1049/iet-epa.2020.0504
www.ietdl.org

Angelo Accetta[1] ✉, *Maurizio Cirrincione*[2], *Marcello Pucci*[1], *Antonino Sferlazza*[3]

[1]*INstitute of Marine engineering (INM), Section of Palermo, National Research Council of Italy (CNR), via Ugo la Malfa 153, Palermo, Italy*
[2]*School of Information Technology, Engineering, Mathematics, and Physics (STEMP), University of the South Pacific (USP), Laucala Campus, Suva, Fiji*
[3]*Engineering Department, University of Palermo, viale delle Scienze, Palermo, Italy*
✉ *E-mail: angelo.accetta@cnr.it*

Abstract: This study proposes a state formulation of the space-vector dynamic model of the Synchronous Reluctance Motor (*SynRM*) considering both saturation and cross-saturation effects. The proposed model adopts the stator currents as state variables and has been theoretically developed in both the rotor and stator reference frames. The proposed magnetic model is based on a flux versus current approach and relies on the knowledge of 11 parameters. Starting from the definition of a suitable co-energy variation function, new flux versus current functions have been initially developed, based on the hyperbolic functions and, consequently, the static and dynamic inductance versus current functions have been deduced. The dynamic inductance functions have been derived so to fulfill the reciprocity conditions. This study presents also a technique for the estimation of the parameters of the proposed magnetic model, which is based on stand-still tests without the need to lock the rotor. The identification process has been performed based on the minimization of a suitably defined error function including the difference between the measured and estimated stator fluxes. The proposed parameter estimation technique has been tested in both numerical simulation and experimentally on a suitably developed test set-up, permitting the experimental validation of the proposed model.

1 Introduction

Synchronous reluctance motors (*SynRMs*) have proved to be a valid alternative to permanent magnet synchronous motors (*PMSMs*) over the last few decades, especially for their robustness, simplicity and lower prices [1–3]. Indeed, they can tolerate short-duration overload, have high dynamical performance over a wide range of speeds, and can be operated in deep flux weakening, which has resulted in several industry applications. In particular, *SynRMs* can operate at an efficiency comparable or higher than that of the induction motor (*IM*), because of the absence of power losses in the rotor, especially when maximum torque per ampere (*MTPA*)) strategies are added into the control strategy of the drive system. However, one of the roadblocks to enhance their dynamical performance is the appropriate development of the dynamical model along with an accurate estimation of the related parameters, which can vary significantly with the saturation of the iron core.

Actually, if non-linear control techniques are to be adopted, the correct modelling of *SynRM* plays an all-important role, e.g. if the input–output feedback linearisation were used, it is well known that its performance would be highly affected by how accurate the model is. In this respect, it is most convenient to write the dynamical model in terms of state variables. This would make it possible the application of linear or non-linear control strategies as well as suitable observers for either speed estimation or implementation of *MTPA* based approaches. For this purpose, the complete flux versus current, or also the current versus flux, characteristics should be fully identified, to include self- and cross-saturation effects [4–6].

In [7], the authors have investigated the effects that non-optimal modelling of the SynRM can have on the dynamic performance of the control. It has been found that neglecting magnetic saturation can severely hamper the dynamic performance of closed-loop control and considering constant inductances lead up to a severe deviation in torque capability prediction. The authors compute inductances look-up tables (LUT) by using finite element method (FEM): even if FEM can give better results in terms of model precision, it lacks generality, since a FEM analysis should be done for a given motor geometry, and it also needs the knowledge of motor constructive elements that are rarely available to the user.

In [8] the authors exploit an offline inductance estimator to obtain a loss minimisation control: the adopted model uses 16 parameters, to be identified through experimental tests. Their inductances equations, however, do not satisfy the reciprocity condition and are not thus suitable to describe the cross-magnetic saturation.

In [9] the authors address the issue of the experimental magnetic characterisation of the flux versus current relationship of IPMs and PM assisted *SynRMs*. In particular, a simplified but effective model of the cross-saturation phenomenon is proposed where the co-energy variation function is divided into three terms, two related to the direct component and one related to the quadrature components of the stator currents.

In [10] the authors present the analysis and mathematical dynamic modelling of *SynRMs*, with the state equations expressed as a function of the stator flux. It should be noted that no magnetic modelling of the machine is included and only simulation results are presented. Moreover, no state formulation of the model as a function of the stator current is proposed.

In [11, 12] the authors present the modelling and vector control of *SynRMs*, taking into consideration the stator iron losses. In [11] the stator iron losses have been modelled by an equivalent resistance in voltage equations, but no self- nor cross-saturation has been treated. Xu *et al.* [12], besides the control, presents also a simplified steady-state *d–q* dynamic model including saturation and iron losses.

A state variable formulation using the space vectors is proposed in [13], where the authors select either the stator flux or the stator current components as state variables. In addition, they develop an in-depth review of the approaches proposed in the literature and show the need of the analytical expression of the inductances versus current, derived from the expressions of the flux versus current components, if stator currents are employed as state

variables. Inductances are modelled as piecewise functions in [14, 15] goes a step forward by including the cross-saturation effects. A further development is achieved in [16] where inductances are modelled with polynomials of 12*th* degree and the coefficients are estimated by using a least-square (LS) method. An enhancement is described in [17], which models inductances with rational functions requiring the estimation of 16 coefficients, but it fails to fulfil the reciprocity conditions. On the other hand, the adoption of the stator flux as state variable leads up to the necessity of using an inductance versus the flux function, which can be obtained with a current versus the flux function. In this respect, the current versus flux can be modelled by using a power function [18], resulting in the development of an inductance versus flux function, although cross-saturation effect is again neglected. In the same fashion, an inverse tangent function has been adopted in [17] to model the inductance: this approach needs only three coefficients with a physical interpretation and, therefore, the fitting procedure is simpler; however, also in this case, cross-saturation effect is neglected. Unlike these works, another approach is presented in [13] by using an augmented power function for fitting the current versus flux relationship. This work uses nine coefficients and considers the cross-saturation. However, since this approach uses the current versus flux relationship, its coefficients cannot be easily interpreted from a physical perspective.

As for the characterisation of *SynRMs*, and the estimation of the model parameters, the common strategy generally requires the *SynRM* to operate at constant speed, with the resulxting need of a prime mover drive controlled in speed in the four quadrants [19]. Another approach is based on the acceleration tests [20], or the injection of large signals at high frequency in standstill conditions [21]. Identification techniques in standstill with zero torque have also been developed in [22, 23]: the background idea lies in applying square voltage waveforms to the direct and quadrature axes circuits of the motor with the effect of identifying the self-saturation parameters separately. Subsequently, two other square voltage waveforms at different frequencies are simultaneously applied to the two axis circuits, to identify the cross-saturation parameters of the model. In particular, a flux versus current function is used in [22], where a linear approximation of the flux is adopted for low current values, whereas for higher values, a linear and inversely proportional function is employed. In this approach, four parameters are used for the self-saturation on each axis and they are estimated with a multiple linear regression (MLR) method. This approach yields the entire flux map, considering also the cross-saturation effect, but does not provide any analytical expression for the cross-saturation flux term. Differently from this work, a current versus flux approach is the base in [23], whose model includes explicitly both the self-saturation and cross-saturation terms like [13]. Specifically, this last work demonstrates that simple polynomials can be used to model inverse functions describing the saturation effect, fulfilling at the same time the reciprocity conditions. This model uses in total nine coefficients, three for describing the self-saturation on each axis and three for the cross-saturation. All these parameters have been estimated by a linear least-squares (LLS) method.

2 Improvements with respect to previous contributions

Recently, in the scientific literature, the mathematical modelling of the magnetic saturation of *SynRMs* has been addressed by using a flux versus current approach, exploiting a mathematical representation with eight coefficients [24]. This mathematical model is based on a combination of linear and exponential terms, and it considers both self-saturation and cross-saturation. In particular, cross-saturation phenomenon has been modelled to fulfil the reciprocity conditions. Starting from the stator flux versus stator current functions, the corresponding expressions of the static and dynamic stator inductances have been deduced, including the cross-saturation dynamic inductances. In [25], a space-vector dynamic model of the *SynRM* has been developed, where the stator currents have been chosen as state variables. The model in [25], expressed in the rotor reference frame, requires the knowledge of the static and dynamic inductances, as presented in [24]. As for the identification of the parameters of the magnetic model in [24], a set of steady-state standstill tests has been devised, not requiring the rotor to be locked in any predefined angular position. Two approaches have been followed. The first minimises an error function of the difference between the measured and estimated stator currents by using a Levenberg–Marquardt algorithm (LMA) [25]. The second minimises a similar error function, dependent on the stator flux error, by using genetic algorithms (GAs) [24]. Both approaches have been assessed in simulation and experimentally on a suitable experimental rig.

This paper is in the framework of [24, 25], but improves them in the following aspects. Like [24, 25], it is based on a flux versus current approach, but the mathematical modelling of the magnetic saturation of *SynRMs* has been entirely rewritten and enhanced with the use of hyperbolic functions. The cross-saturation flux term has been obtained based on the preliminary definition of a suitable co-energy variation function. This co-energy variation function has been created to properly represent the physical phenomenon of the cross-saturation in certain operating points, as fully explained in the following. Starting from the definition of the co-energy function, the static and dynamic inductance functions have been defined, including the cross-saturation term. In particular, the co-energy function has been defined so that the cross-saturation inductance can fulfil the reciprocity conditions. The entire magnetic model requires the knowledge of 11 parameters: 6 describing the self-saturation on the direct and quadrature axis, and 5 describing the cross-saturation. A set of steady-state standstill test has been devised to identify the entire set of the 11 parameters of the model, not requiring the rotor to be locked in any predefined angular position. The method is based on the minimisation of a suitably defined cost function based on the error between the stator flux components, respectively, estimated by the model and experimentally measured. In particular, GAs have been exploited to solve the optimisation problem, as in [24].

This paper, besides the mathematical model of the magnetic saturation of the *SynRM*, presents also a further improvement, with respect to [25], of the space-vector dynamic model of the *SynRM* in state form, assuming the stator currents as state variables. Specifically, the entire formulation of this model has been expressed also in the stator reference frame, that proves particularly useful for developing non-linear controllers and observers.

The parameters of the model have been experimentally identified on a suitably developed test set-up, and the proposed model has been fully assessed.

As for the number of parameters required by the model, the proposed model requires three parameters to describe the self-saturation on each axis, equal to those required by Hinkkanen *et al.* [23] and one less than those required by Bedetti *et al.* [22]. Moreover, the proposed model requires five parameters to describe the cross saturation, whereas Hinkkanen *et al.* [23] require three parameters and Bedetti *et al.* [22] do not present a mathematical model of the cross-saturation. The reason why the proposed model requires a higher number of parameters than Hinkkanen *et al.* [23] is that it better describes the reduction of the cross-saturation effect in the deep saturation region (as clearly shown in Fig. 2 of [4]). As for the complexity, the proposed model is certainly more involved than that in [22], but it is more accurate since the non-linearity of the curve can be much better tracked with hyperbolic functions, especially on the direct axis and in correspondence of the knee of the saturation curve. The proposed model presents a complexity that is comparable to that of the model in [23]. It should be noted that the main reason for adopting a current versus flux approach is that a simple polynomial function can interpolate the experimental points. On the contrary, the interpolating flux versus current function is inherently more complex. The flux versus current approach reflects better the physics of the phenomenon, since inside the machine the current is the cause and the magnetic flux is the effect. As for the computational requirement, the following considerations can be made. In general, the dynamic model is used off-line on a regular PC for simulating the behaviour of the machine before the experimental tests. From this point of view, a

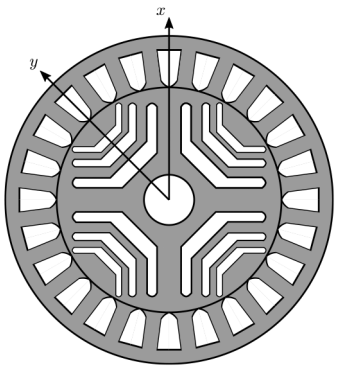

Fig. 1 *Cross-section of the SynRM*

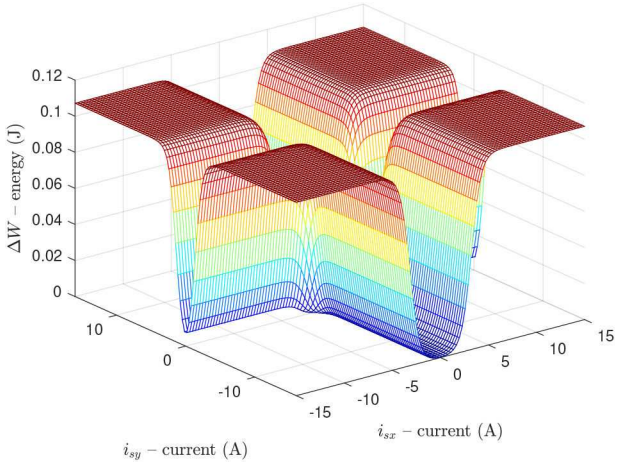

Fig. 2 *Co-energy variation surface versus i_{sx}, i_{sy}*

Table 1 Rated data of the *SynRM*

rated power, kW	2.2
rated voltage, V	380
rated frequency, Hz	50
pole-pairs	2
rated speed, rpm	1500
rated current, A RMS	5.5
rated torque, Nm	14

higher computational time is certainly not a big problem, given the very high computational power offered by modern PCs. In general, the dynamic model can be even suitably exploited to develop non-linear control techniques or observers. As for the on-line implementation on embedded platforms (DSPs) of the non-linear functions describing the model, linearly interpolated look-up tabled can easily be used, ensuring at the same time good accuracy and low computational demand. It should be further noted that hyperbolic functions are just combination of simple exponentials, while trigonometric functions are combination of complex exponential, which are far more complex and computationally demanding. Furthermore, the hyperbolic notation permits certainly a more compact form of the equations and a better elegance of the mathematical representation.

3 Space-vector dynamic model of *SynRM* motor

Fig. 1 shows the cross-section of a *SynRM*. The space-vector dynamic model described in the following is based on the assumption of fundamental of the magnetomotive force (MMF), meaning that all its space harmonics are neglected. In the following, the model has been initially developed in the rotor reference frame. If the stator flux space-vector $\boldsymbol{\Psi}_s^r = \psi_{sx} + j\psi_{sy}$ is chosen as state vector variable, the classic space-vector equations of the *SynRM* expressed in the rotor reference frame with the x axis aligned in the direction of minimum reluctance can be obtained, written in complex form:

$$\frac{\mathrm{d}\boldsymbol{\Psi}_s^r}{\mathrm{d}t} = \boldsymbol{u}_s^r - R_s\boldsymbol{i}_s^r - \omega_r j\boldsymbol{\Psi}_s^r \tag{1}$$

and in scalar form, after decomposing on the direct x -axis and quadrature y-axis:

$$\begin{aligned}\frac{\mathrm{d}\psi_{sx}}{\mathrm{d}t} &= u_{sx} - R_s i_{sx} + \omega_r\psi_{sy}\\ \frac{\mathrm{d}\psi_{sy}}{\mathrm{d}t} &= u_{sy} - R_s i_{sy} - \omega_r\psi_{sx}\end{aligned} \tag{2}$$

where $\boldsymbol{u}_s^r$ and $\boldsymbol{i}_s^r$ are the stator voltage and current space-vectors, respectively, R_s is the stator resistance and ω_r is the angular speed of the rotor in electrical angles. The ^{r} superscript indicates that all variables are written in the rotor reference frame.

3.1 Magnetic characterisation of the SynRM

The magnetic characteristics of the *SynRM* have been deduced by using a flux versus current approach rather than the current versus flux approach, because it is more consistent with the physics of the real system. The problem of finding the stator flux variation on the direct and the quadrature axes due to the cross-saturation has been addressed by adopting a variable-separation method [4, 26]. In particular, the co-energy variation caused by the cross-saturation has been expressed as a product of two non-linear functions, each depending on the stator current component of only one axis

$$\begin{aligned}\Delta W' &= F(i_{sx})G(i_{sy})\\ &= \frac{\gamma}{4}\left[\tanh\left(\frac{(i_{sx} - \mu_1\mathrm{sign}(i_{sx}))}{\sigma_1}\right)\cdot\mathrm{sign}(i_{sx}) + 1\right]\\ &\cdot\left[\tanh\left(\frac{(i_{sy} - \mu_2\mathrm{sign}(i_{sy}))}{\sigma_2}\right)\cdot\mathrm{sign}(i_{sy}) + 1\right]\end{aligned} \tag{3}$$

Fig. 2 shows the co-energy variation surface $\Delta W'$ in (3) versus the stator current components i_{sx}, i_{sy}, related to the *SynRM* under test, where the parameters are shown in Table 1. It can be observed that the co-energy variation is null for zero value of any stator current component, and it saturates to a maximum positive (negative) value with increasing values of the stator current components of the same (different) sign.

The physical explanation of this model is explained in the following. Equation (3) describes the co-energy variation function due to the cross-saturation, expressed as the product of two functions, one depending only on i_{sx} and the other depending only on i_{sy}. This last condition is very important since it permits the reciprocity conditions (8c) to be properly fulfilled. The mathematical formulation has been created based on the analysis of Fig. 2 in [4]. This last figure shows that ψ_{sx} reduces for increasing values of the current i_{sy}. Moreover, for a given value of i_{sx}, the amount of reduction of ψ_{sx} depends on the absolute value of i_{sy}, being independent of its sign. The higher the absolute value of i_{sy}, the higher the flux reduction on the x-axis. In addition, the same figure shows that the flux variation on the x-axis is null for zero value of i_{sx}, very small for high values of i_{sx}, while it presents a maximum for a certain intermediate range of i_{sx}. These considerations suggest that the flux variation on the x axis should be weighted with a function of i_{sx} presenting a bell shape. A possible choice would be the Gaussian, but this function does not present a known primitive, necessary to compute the co-energy function (4). Another function choice with a bell shape, which has been adopted here, is the $1/\cosh^2(\cdot)$ function, centred on μ_1 and characterised by a rate of change related to σ_1, whose primitive is well known as the $\tanh(\cdot)$ function. Finally, this formulation permits the reciprocity conditions to be properly fulfilled, since the cross-saturation dynamic inductances on the two axes are equal and

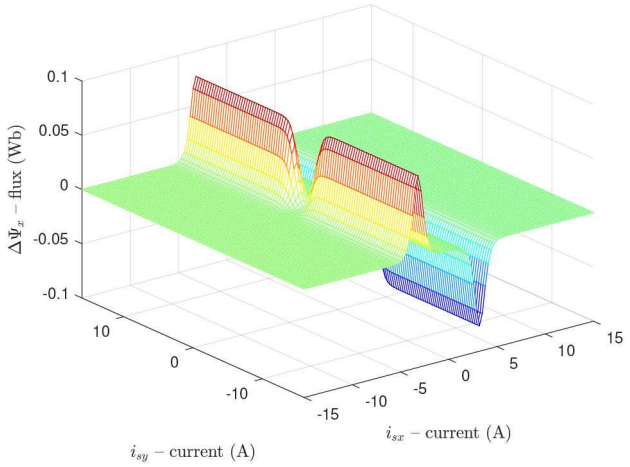

Fig. 3 *Stator flux variation $\Delta\Psi_x$ versus i_{sx}, i_{sy} caused by cross-saturation*

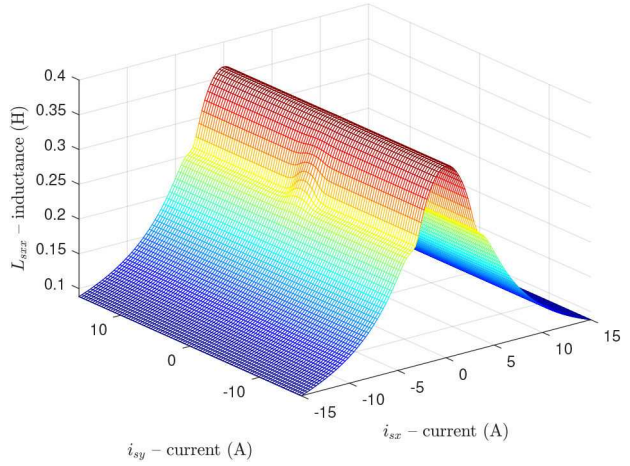

Fig. 4 *Static inductance L_{sxx} versus i_{sx}, i_{sy}*

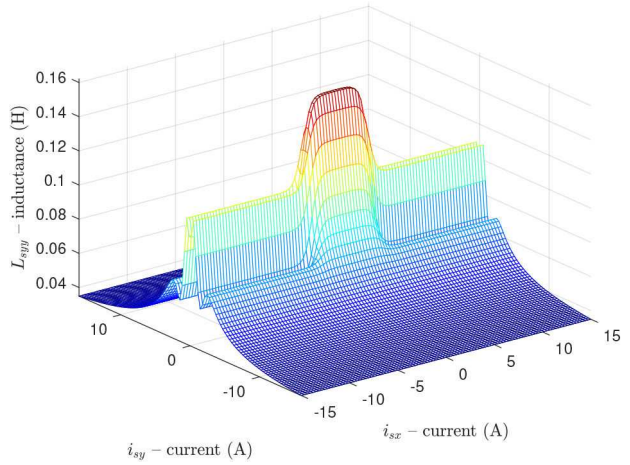

Fig. 5 *Static inductance L_{syy} versus i_{sx}, i_{sy}*

related to the product of two $1/\cosh^2(\cdot)$ functions. Based on the above considerations, the choice of the representation of the co-energy function as the product of two $\tanh(\cdot)$ functions reveals ideal to properly represent the physical behaviour of the system.

Starting from the expression (3), the flux variation terms caused by the cross-saturation have been derived as follows:

$$\frac{\partial \Delta W'}{\partial i_{sx}} = F'(i_{sx})G(i_{sy}) = -\Delta\Psi_{sx} \tag{4a}$$

$$\frac{\partial \Delta W'}{\partial i_{sy}} = F(i_{sx})G'(i_{sy}) = -\Delta\Psi_{sy} \tag{4b}$$

The self-saturation terms have been devised as the sum of two terms, the first based on a *tanh* function plus a linear term. As a result, the expressions of the flux terms on the direct and quadrature axes are the following equations:

$$\Psi_{sx} = \alpha_1 \tanh(\beta_1 i_{sx}) + \eta_1 i_{sx} + -\frac{\gamma}{4}\operatorname{sign}(i_{sx})\frac{\tanh\left(\frac{(i_{sy}-\mu_2\operatorname{sign}(i_{sy}))}{\sigma_2}\right)\cdot\operatorname{sign}(i_{sy})+1}{\sigma_1\cosh^2\left(\frac{(i_{sx}-\mu_1\operatorname{sign}(i_{sx}))}{\sigma_1}\right)} \tag{5a}$$

$$\Psi_{sy} = \alpha_2 \tanh(\beta_2 i_{sy}) + \eta_2 i_{sy} + -\frac{\gamma}{4}\operatorname{sign}(i_{sy})\frac{\tanh\left(\frac{(i_{sx}-\mu_1\operatorname{sign}(i_{sx}))}{\sigma_1}\right)\cdot\operatorname{sign}(i_{sx})+1}{\sigma_2\cosh^2\left(\frac{(i_{sy}-\mu_2\operatorname{sign}(i_{sy}))}{\sigma_2}\right)} \tag{5b}$$

Fig. 3 shows the stator flux variation $\Delta\Psi_x$ versus i_{sx}, i_{sy} (3rd terms in (5)) caused by cross-saturation related to the *SynRM* under test, whose parameters are shown in Table 1. It can be observed that $\Delta\Psi_x$ is negative for positive values of i_{sx}, changing its sign with the sign of i_{sx}. On the contrary, $\Delta\Psi_x$ does not change its sign with the sign of i_{sy}, depending only on its absolute value. Moreover, $\Delta\Psi_x$ varies with a tanh function of i_{sy} with a null value for $i_{sy,0} = \mu_2\operatorname{sign}(i_{sy,0})$, weighted with a $1/\cosh^2$ function of i_{sx} with a maximum for $i_{sx,0} = \mu_1\operatorname{sign}(i_{sx,0})$; as a result, the cross-saturation flux variation is null for $i_{sx} = 0$, and tends to zero for $i_{sx} \to \infty$ presenting a maximum for a non-null value of i_{sx}. Furthermore, it represents the cross-saturation phenomenon better than [24, 25], where $\Delta\Psi_x$ increases with i_{sy} and is maximum for null value of i_{sx} while reducing quickly for increasing values of it (see Fig. 8 in [24]). Finally, in [24] $\Delta\Psi_x$ does not change its sign with i_{sx}, differently from what is represented in Fig. 3.

Starting from the equations of the stator flux components, the relationship between the vectors of the stator flux and current is the following equation:

$$\boldsymbol{\Psi}_s^r = \begin{bmatrix} L_{sxx} & 0 \\ 0 & L_{syy} \end{bmatrix} \boldsymbol{i}_s^r = \boldsymbol{L}_s \boldsymbol{i}_s^r \tag{6}$$

where the direct (x) and quadrature (y) static inductance components (also called synchronous inductances) can be deduced, from the stator flux components in (4), as

$$L_{sxx} = \frac{\Psi_{sx}}{i_{sx}} = \frac{\alpha_1\tanh(\beta_1 i_{sx})}{i_{sx}} + \eta_1 + -\frac{\gamma}{4}\frac{\operatorname{sign}(i_{sx})}{i_{sx}}\frac{\tanh\left(\frac{(i_{sy}-\mu_2\operatorname{sign}(i_{sy}))}{\sigma_2}\right)\cdot\operatorname{sign}(i_{sy})+1}{\sigma_1 i_{sx}\cosh^2\left(\frac{(i_{sx}-\mu_1\operatorname{sign}(i_{sx}))}{\sigma_1}\right)} \tag{7a}$$

$$L_{syy} = \frac{\Psi_{sy}}{i_{sy}} = \frac{\alpha_2\tanh(\beta_2 i_{sy})}{i_{sy}} + \eta_2 + -\frac{\gamma}{4}\frac{\operatorname{sign}(i_{sy})}{i_{sy}}\frac{\tanh\left(\frac{(i_{sx}-\mu_1\operatorname{sign}(i_{sx}))}{\sigma_1}\right)\cdot\operatorname{sign}(i_{sx})+1}{\sigma_2 i_{sy}\cosh^2\left(\frac{(i_{sy}-\mu_2\operatorname{sign}(i_{sy}))}{\sigma_2}\right)} \tag{7b}$$

Figs. 4 and 5 show the stator static inductances L_{sxx}, L_{syy} versus i_{sx}, i_{sy}, related to the *SynRM* under test, whose parameters are shown in Table 1, and plotted on the basis of (7). Fig. 4 clearly shows that L_{sxx} varies mainly with i_{sx}, while it is only moderately influenced by i_{sy}. This is to be expected, considering that the magnetic circuit on the x-axis lies mainly in iron, while that on the y-axis presents both iron and flux barriers. Starting from its maximum value, L_{sxx} reduces quickly with i_{sx} because of the saturation of the iron path on the x-axis. In a certain range of values of i_{sx}, for high absolute values of i_{sy} (independently of its sign), the inductance is further reduced, since the load causes an increased saturation of the iron core. Above some values of i_{sx}, the magnetic

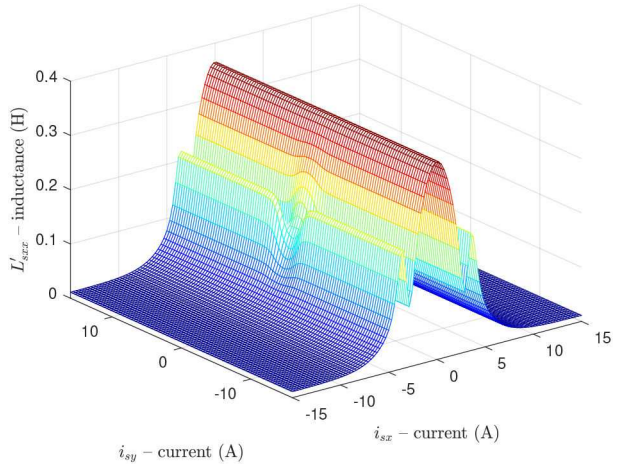

Fig. 6 *Dynamic inductance L'_{sxx} versus i_{sx}, i_{sy}*

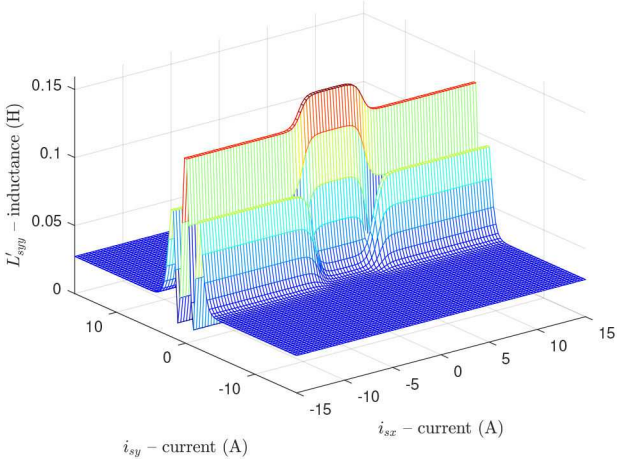

Fig. 7 *Dynamic inductance L'_{syy} versus i_{sx}, i_{sy}*

circuit has been already so saturated that the load has a minimum impact, independently of the amplitude of i_{sy}. On the contrary, Fig. 5 clearly shows that L_{syy} varies significantly with both i_{sx} and i_{sy}. In particular, it reduces quickly with i_{sy} because of the rapid saturation of the iron part of the circuit on the y-axis, as expected. At the same time, even small increases of i_{sx} lead the magnetic circuit on the quadrature axis to saturation. Indeed, if i_{sy} is small in absolute, even a small positive increase of i_{sx} causes the magnetic circuit to achieve full saturation, with consequent sudden reduction of the inductance.

Starting from the stator flux components in (5), the direct (x) and quadrature (y) dynamic inductance components can be deduced as follows:

(see (8a))

(see (8b))

(see (8c))

Figs. 6–8 show the stator dynamic inductances (also called incremental inductances) L'_{sxx}, L'_{syy} and L'_{sxy} versus i_{sx}, i_{sy}, for the *SynRM* under test, whose parameters are shown in Table 1, and plotted on the basis of (8). Figs. 6 and 7 clearly show that the shapes of the dynamic self-inductances are very similar to the corresponding ones of the static self-inductance. It can be further observed that the effect of the cross-saturation is more apparent in the dynamic inductances than in the static ones.

Fig. 8 shows that the dynamic cross-saturation inductance presents a polar symmetry, as expected. There are specific current ranges in which the cross-saturation inductance is non-null, with maxima values obtained for specific values of i_{sx}, i_{sy}, while elsewhere it is close to zero because of the full saturation of the magnetic circuit. When i_{sx} and i_{sy} present the same sign, then the cross-saturation dynamic inductance assumes negative values, while when they present opposite signs, it presents positive values, accordingly with the analysis in [27].

The comparison of Figs. 4–8 with the corresponding ones in [24, 25] highlights the different approach in modelling the cross-saturation phenomenon.

3.2 State formulation based on the stator currents

Finally, the complete space-vector dynamic model of the *SynRM* in state form, selecting the stator currents as state variables and expressed in the rotor reference frame, can be written as

$$\frac{\mathrm{d}\boldsymbol{i}_s^r}{\mathrm{d}t} = (\boldsymbol{L}'_s)^{-1}(\boldsymbol{u}_s^r - R_s\boldsymbol{i}_s^r - \omega_r \boldsymbol{j}\boldsymbol{L}_s\boldsymbol{i}_s^r) \tag{9}$$

where the $\boldsymbol{L}'_s$ is the Jacobian matrix of the stator flux function defined in (6). This matrix is symmetrical for the reciprocity condition and can be related to the derivative of the stator flux as follows:

$$\frac{\mathrm{d}\boldsymbol{\Psi}_s^r}{\mathrm{d}t} = \frac{\mathrm{d}\boldsymbol{\Psi}_s^r}{\mathrm{d}\boldsymbol{i}_s^r}\frac{\mathrm{d}\boldsymbol{i}_s^r}{\mathrm{d}t} = \begin{bmatrix} L'_{sxx} & L'_{sxy} \\ L'_{sxy} & L'_{syy} \end{bmatrix}\frac{\mathrm{d}\boldsymbol{i}_s^r}{\mathrm{d}t} = \boldsymbol{L}'_s\frac{\mathrm{d}\boldsymbol{i}_s}{\mathrm{d}t} \tag{10}$$

and its components are defined in (8).

It can be observed that the dynamic inductance matrix presents, different from the static one, non-zero cross-coupling terms. Such coupling terms are responsible for the cross-saturation. The cross-coupling terms are equal, in accordance with the respect of the reciprocity conditions. Finally, the inverse of the stator dynamic matrix in (9) is defined as follows:

$$(\boldsymbol{L}'_s)^{-1} = \frac{1}{L'_{sxx}L'_{syy} - L'^{2}_{sxy}}\begin{bmatrix} L'_{syy} & -L'_{sxy} \\ -L'_{sxy} & L'_{sxx} \end{bmatrix} \tag{11}$$

The definition of the dynamic model in (9), where the dynamic inductances are defined in (8), is one of the major contribution of [25]. Fig. 9, describing (9), shows the block diagram of the space-vector model of the *SynRM*, including both self- and cross-saturation phenomena, expressed in the rotor reference frame.

$$L'_{sxx} = \frac{\mathrm{d}\Psi_{sx}}{\mathrm{d}i_{sx}} = \frac{\alpha_1\beta_1}{\cosh^2(\beta_1 i_{sx})} + \eta_1 + \frac{\gamma}{2\sigma_1^2}\frac{\mathrm{sign}(i_{sx})\tanh\left(\frac{(i_{sx}-\mu_1\mathrm{sign}(i_{sx}))}{\sigma_1}\right)\left[\tanh\left(\frac{(i_{sy}-\mu_2\mathrm{sign}(i_{sy}))}{\sigma_2}\right)\cdot\mathrm{sign}(i_{sy})+1\right]}{\cosh^2\left(\frac{(i_{sx}-\mu_1\mathrm{sign}(i_{sx}))}{\sigma_1}\right)} \tag{8a}$$

$$L'_{syy} = \frac{\mathrm{d}\Psi_{sy}}{\mathrm{d}i_{sy}} = \frac{\alpha_2\beta_2}{\cosh^2(\beta_2 i_{sy})} + \eta_2 + \frac{\gamma}{2\sigma_2^2}\frac{\mathrm{sign}(i_{sy})\tanh\left(\frac{(i_{sy}-\mu_2\mathrm{sign}(i_{sy}))}{\sigma_2}\right)\left[\tanh\left(\frac{(i_{sx}-\mu_1\mathrm{sign}(i_{sx}))}{\sigma_1}\right)\cdot\mathrm{sign}(i_{sx})+1\right]}{\cosh^2\left(\frac{(i_{sy}-\mu_2\mathrm{sign}(i_{sy}))}{\sigma_2}\right)} \tag{8b}$$

$$L'_{sxy} = \frac{\mathrm{d}\Psi_{sx}}{\mathrm{d}i_{sy}} = L'_{syx} = \frac{\mathrm{d}\Psi_{sy}}{\mathrm{d}i_{sx}} = -\frac{\gamma\mathrm{sign}(i_{sx})\mathrm{sign}(i_{sy})}{4\sigma_1\sigma_2\cosh^2\left(\frac{(i_{sx}-\mu_1\mathrm{sign}(i_{sx}))}{\sigma_1}\right)\cosh^2\left(\frac{(i_{sy}-\mu_2\mathrm{sign}(i_{sy}))}{\sigma_2}\right)} \tag{8c}$$

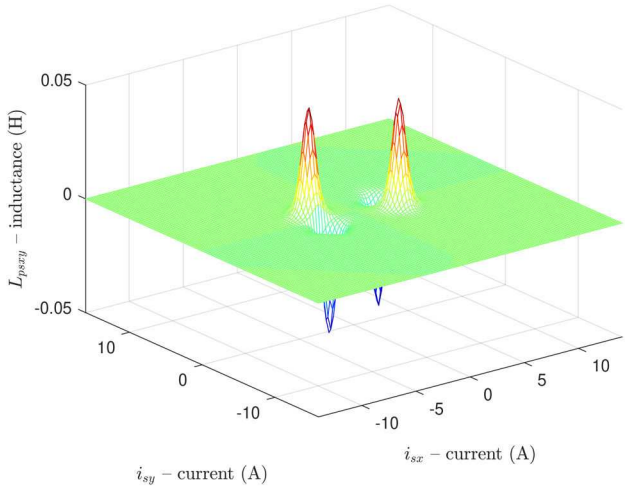

Fig. 8 *Dynamic inductance L'_{sxy} versus i_{sx}, i_{sy}*

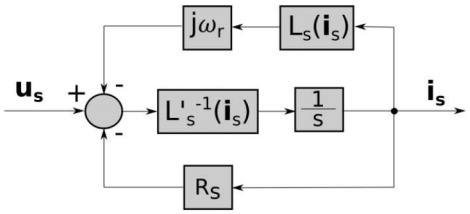

Fig. 9 *Block diagram of space-vector SynRM model in the rotor reference frame*

As a major theoretical contribution of this paper, the proposed space-vector model in (9) has been expressed also in the stator reference frame. If (9) is vector-rotated from the rotor reference frame (r) to the stator reference frame (s), the state formulation of the dynamic model of the *SynRM* can be found. Being $\boldsymbol{T}$ the transformation matrix from the stator to the rotor reference frame

$$\boldsymbol{T} = \begin{bmatrix} \cos\theta_r & \sin\theta_r \\ -\sin\theta_r & \cos\theta_r \end{bmatrix}$$

Equation (9) can be written as

$$\boldsymbol{L}'_s \frac{\mathrm{d}}{\mathrm{d}t}(\boldsymbol{T}\boldsymbol{i}^s_s) = \boldsymbol{T}\boldsymbol{u}^s_s - R_s\boldsymbol{T}\boldsymbol{i}^s_s - \omega_r \boldsymbol{j}\boldsymbol{L}_s\boldsymbol{T}\boldsymbol{i}^s_s \tag{12}$$

where $\boldsymbol{j}$, matricial equivalent to imaginary unit, is defined as

$$\boldsymbol{j} = \begin{bmatrix} 0 & -1 \\ 1 & 0 \end{bmatrix}$$

Defining the $\boldsymbol{R}$ matrix as

$$\boldsymbol{R} = \begin{bmatrix} \sin\theta_r & -\cos\theta_r \\ \cos\theta_r & \sin\theta_r \end{bmatrix} = \boldsymbol{j}\boldsymbol{T}$$

it results that

$$\frac{\mathrm{d}\boldsymbol{T}}{\mathrm{d}t} = -\omega_r\boldsymbol{R} = -\omega_r\boldsymbol{j}\boldsymbol{T}$$

therefore, (12) can be written as

$$\begin{aligned} \frac{\mathrm{d}\boldsymbol{i}^s_s}{\mathrm{d}t} &= (\boldsymbol{L}'_s\boldsymbol{T})^{-1}\left[\boldsymbol{T}\boldsymbol{u}^s_s - R_s\boldsymbol{T}\boldsymbol{i}^s_s + \omega_r(\boldsymbol{L}'_s\boldsymbol{R} - \boldsymbol{j}\boldsymbol{L}_s\boldsymbol{T})\boldsymbol{i}^s_s\right] = \\ &= (\boldsymbol{L}'_s\boldsymbol{T})^{-1}\boldsymbol{T}(\boldsymbol{u}^s_s - R_s\boldsymbol{i}^s_s) + \omega_r(\boldsymbol{L}'_s\boldsymbol{T})^{-1}(\boldsymbol{L}'_s\boldsymbol{R})\boldsymbol{i}^s_s + \\ &\quad -\omega_r(\boldsymbol{L}'_s\boldsymbol{T})^{-1}(\boldsymbol{j}\boldsymbol{L}_s\boldsymbol{T})\boldsymbol{i}^s_s \end{aligned} \tag{13}$$

All the matrices defined in (13) are given as below:

$$(\boldsymbol{L}'_s\boldsymbol{T})^{-1} = \frac{1}{L'_{sxx}L'_{syy} - L'^2_{sxy}} \begin{bmatrix} L'_{sxy}\sin\theta_r + L'_{syy}\cos\theta_r & -L'_{sxx}\sin\theta_r - L'_{sxy}\cos\theta_r \\ L'_{syy}\sin\theta_r - L'_{sxy}\cos\theta_r & -L'_{sxy}\sin\theta_r + L'_{sxx}\cos\theta_r \end{bmatrix}$$

$$(\boldsymbol{L}'_s\boldsymbol{R}) = \begin{bmatrix} L'_{sxx}\sin\theta_r + L'_{sxy}\cos\theta_r & L'_{sxy}\sin\theta_r - L'_{sxx}\cos\theta_r \\ L'_{sxy}\sin\theta_r + L'_{syy}\cos\theta_r & L'_{syy}\sin\theta_r - L'_{sxy}\cos\theta_r \end{bmatrix}$$

$$(\boldsymbol{j}\boldsymbol{L}_s\boldsymbol{T}) = \begin{bmatrix} L_{syy}\sin\theta_r & -L_{syy}\cos\theta_r \\ L_{sxx}\cos\theta_r & L_{sxx}\sin\theta_r \end{bmatrix}$$

$$(\boldsymbol{L}'_s\boldsymbol{T})^{-1}\boldsymbol{T} = \frac{1}{2\left(L'_{sxx}L'_{syy} - L'^2_{sxy}\right)}$$

$$\begin{bmatrix} \left(L'_{syy} + L'_{sxx}\right) + \left(L'_{syy} - L'_{sxx}\right)\cos 2\theta_r + \cdots \\ +2L'_{sxy}\sin 2\theta_r \\ \left(L'_{syy} - L'_{sxx}\right)\sin 2\theta_r - 2L'_{sxy}\cos 2\theta_r \end{bmatrix}$$

$$\begin{bmatrix} \left(L'_{syy} - L'_{sxx}\right)\sin 2\theta_r - 2L'_{sxy}\cos 2\theta_r \\ \left(L'_{syy} + L'_{sxx}\right) - \left(L'_{syy} - L'_{sxx}\right)\cos 2\theta_r + \cdots \\ -2L'_{sxy}\sin 2\theta_r \end{bmatrix}$$

$$(\boldsymbol{L}'_s\boldsymbol{T})^{-1}(\boldsymbol{L}'_s\boldsymbol{R}) = \boldsymbol{j}$$

(see equation below)

It can be observed that several terms depending on twice the rotor angle appear, that are typical of the main magnetic saliency of such machines and are present also in the classic model of the PMSM expressed in the stationary reference frame.

It is to be further noted that, if the saturation of the iron core is neglected, the dynamic inductance matrix coincides with the static one and the model identifies with the classic dynamic model of the synchronous machine, where the permanent magnet flux term is null.

4 Parameter estimation technique

The parameter estimation requires three tests at standstill under different supply conditions, as performed in [22]. In all of the three tests, a simple hysteresis current controller has been adopted, regulating the stator current direct and quadrature components in the rotor reference frame. Fig. 10 shows the block diagram of the parameter estimation technique.

As for the x-axis controller, the control law can be written as follows:

$$(\boldsymbol{L}'_s\boldsymbol{T})^{-1}(\boldsymbol{j}\boldsymbol{L}_s\boldsymbol{T}) = \frac{1}{2\left(L'_{sxx}L'_{syy} - L'^2_{sxy}\right)} \begin{bmatrix} \left(L_{syy}L'_{syy} - L_{sxx}L'_{sxx}\right)\sin 2\theta_r + L_{syy}L'_{sxy}(1 - \cos 2\theta_r) - L_{sxx}L'_{sxy}(1 + \cos 2\theta_r) \\ -\left(L_{syy}L'_{sxy} + L_{sxx}L'_{sxy}\right)\sin 2\theta_r + L_{syy}L'_{syy}(1 - \cos 2\theta_r) + L_{sxx}L'_{sxx}(1 + \cos 2\theta_r) \\ -\left(L_{syy}L'_{sxy} + L_{sxx}L'_{sxy}\right)\sin 2\theta_r - L_{syy}L'_{syy}(1 + \cos 2\theta_r) - L_{sxx}L'_{sxx}(1 - \cos 2\theta_r) \\ -\left(L_{syy}L'_{syy} - L_{sxx}L'_{sxx}\right)\sin 2\theta_r + L_{syy}L'_{sxy}(1 + \cos 2\theta_r) - L_{sxx}L'_{sxy}(1 - \cos 2\theta_r) \end{bmatrix}$$

$$u_{sx,\mathrm{ref}}(k)=\begin{cases}U_{sx,0} & \text{if } i_{sx}(k)<-i_{sx,\max}\\ u_{sx,\mathrm{ref}}(k-1) & \text{if } |i_{sx}(k)|\le i_{sx,\max}\\ -U_{sx,0} & \text{if } i_{sx}(k)>i_{sx,\max}\end{cases}$$

where $U_{sx,0}$ is the constant value of the voltage to be generated by the inverter, $i_{sx,\max}$ is the limit value allowed for the current to flow in the stator windings, k is the sampled time interval. Such a controller prevents the stator current from overcoming the allowed maximum value. As for the position of the rotor reference frame, the value of the initial angle of the x-axis should be estimated under the assumption that the rotor will not move significantly during the test. If the motor is installed in such a way that the rotor position cannot be modified, the DC current can be injected into the desired direction before the test, so that the magnetic field is spatially aligned with the rotor. Alternatively, the initial x axis position could be found by using a signal-injection method, without any resulting rotor movement.

During *test 1*, only the x-axis is supplied, while the y-axis voltage is null. The measured currents are acquired and post-processed by the identification algorithm to estimate the parameters α_1, β_1 and η_1 related to the self-saturation effects on the x-axis; the other parameters are not considered in this test because $i_{sy}=0$, therefore, Ψ_{sy} could be assumed to be zero, and also the third term of (5a) can be neglected since it takes into consideration the cross-saturation effects. During *test 2*, only the y-axis is supplied, while the x-axis voltage is null. In this case, the parameters α_2, β_2 and η_2 are estimated related to the self-saturation effects on the y-axis: also in this case, only these three parameters are considered since $i_{sx}=0$.

The cost function to be minimised depends on the error between the measured and estimated stator flux x, y components. In this case, the stator flux components have been estimated on-line on the basis of (1), where the state variable is the stator flux space-vector. Such equations describe the so-called voltage model, expressed in the rotor reference frame. The cost functions are defined by (14a) for *test 1* and (14b) for *test 2*

$$S_1(\boldsymbol{\rho}_1,k)=\frac{1}{N}\sqrt{\sum_{k=1}^{N}\left(\Psi_{sx}(k)-\hat{\Psi}_{sx}(k)\right)^2} \tag{14a}$$

$$S_2(\boldsymbol{\rho}_2,k)=\frac{1}{N}\sqrt{\sum_{k=1}^{N}\left(\Psi_{sy}(k)-\hat{\Psi}_{sy}(k)\right)^2} \tag{14b}$$

where N is the total number of samples supplied to the algorithm, $\boldsymbol{\rho}_1=[\alpha_1,\beta_1,\eta_1]$ and $\boldsymbol{\rho}_2=[\alpha_2,\beta_2,\eta_2]$ are the parameters vectors, and Ψ_{sx}, Ψ_{sy} and $\hat{\Psi}_{sx}$, $\hat{\Psi}_{sy}$ are the direct and quadrature components of the stator fluxes, respectively, measured and estimated by mathematical model (1) using the computed values of the parameters.

Remark 1: The so-called measured stator fluxes components are estimated quantities themselves (even if estimated on-line on the DSP); they have been obtained by integrating (2) with the measured values of u_{sx}, u_{sy}, i_{sx} and i_{sy}, and using the rated value of R_s. Moreover, the condition $\omega_r=0$ has been considered because during these tests the angular speed of the machine is zero. There are two sources of errors in the experimental estimation of the stator flux x, y components.

The minimisation of the cost functions (14) has been carried out by means of the *GAs*, since the problem is not linear, and therefore, it is not possible to solve it by convex optimisation. In particular, the GA of MATLAB$^{\mathrm{TM}}$ has been used. The *GA* is an evolutionary algorithm that, starting from a generic initial condition, generates different sets of parameter vector $\boldsymbol{\rho}_{ji}$, $j=1,2$, and $i=1,2,\ldots,M$, under the linear constraint $\boldsymbol{\rho}_{\inf}<\boldsymbol{\rho}_i<\boldsymbol{\rho}_{\sup}$ (the number of generated sets M is called the number of individuals for each generation). Afterwards, the algorithm computes the cost function (14) associated with each set $\boldsymbol{\rho}_i$. At each iteration, the algorithm selects the best vector $\boldsymbol{\rho}_i$ and generates a new set of parameters

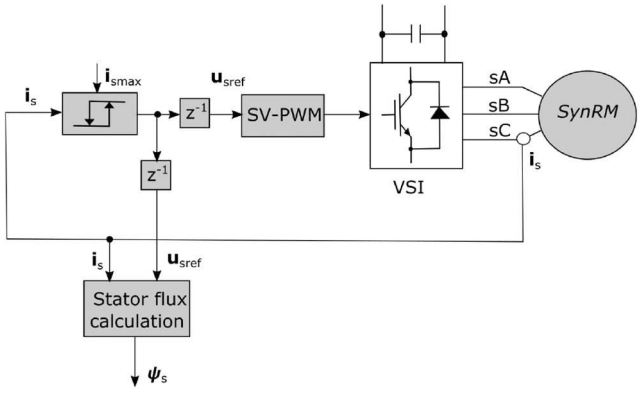

Fig. 10 *Block diagram of the adopted parameter estimation scheme*

including the best one of the precedent generation: this represents the new generation. This cycle continues until the algorithm finds a set of parameters such that the cost function (14) is less that a fixed quantity chosen by design or after a maximum number of generations. For the case under study, the following parameters have been used: $M=30$, $\boldsymbol{\rho}_{\inf}=[0.1\ 0.1\ 0.1]$, $\boldsymbol{\rho}_{\sup}=[2\ 2\ 2]$, and the stopping criteria has been fixed by choosing the maximum number of generations equal to 50 (see [28] for further details on GAs). Moreover, the third parameter of $\boldsymbol{\rho}$ has been scaled by 100, such that all parameters range in comparable intervals, avoiding numerical issues due to a wrong conditioning of the optimisation.

During *test 3*, both the x and the y axes are simultaneously supplied to consider the entire range of the i_{sx}, i_{sy} currents. To this aim, voltage square waveforms on the two axes have been chosen with frequencies multiple of each other. In this case, the parameters γ, μ_1, μ_2, σ_1 and σ_2, related to the cross-saturation effects, are estimated on the basis of the minimisation of the following quadratic error, by combining the flux errors on both the direct and the quadrature axes:

$$S(\boldsymbol{\rho}_3,k)=\frac{1}{N}\sqrt{\sum_{k=1}^{N}\left[\Psi_{sx}(k)-\hat{\Psi}_{sx}(k)\right]^2+\left[\Psi_{sy}(k)-\hat{\Psi}_{sy}(k)\right]^2} \tag{15}$$

GAs have been used as described above, but with the following parameters: $M=30$, $\boldsymbol{\rho}_{\inf}=[0,03\ 0,03\ 0,03\ 0,03\ 0,03]$, $\boldsymbol{\rho}_{\sup}=[1\ 1\ 1\ 1\ 1]$, and the stopping criteria has been fixed by choosing the maximum number of generations equal to 50. Also, in this case, some parameters have been scaled by constant factors such that all parameters range in comparable intervals. In particular, parameter γ has been multiplied by 10, while μ_1 and μ_2 have been divided by 10.

At the end of the three tests, all the 11 parameters of the model have been estimated. The set of final values of the estimated parameters as obtained at the end of the identification process is shown in Table 1.

5 Test set-up

The adopted test set-up has been arranged with a *SynRM* motor model ABB 3GAL092543-BSB whit rated data shown in Table 1. The motors have been supplied by a voltage source inverter (*VSI*) with insulated gate bipolar transistor (IGBT) modules, model Semikron SMK 50 GB 123, driven by a space-vector pulse-width modulation (SV-PWM) technique with PWM frequency set to 5 kHz. The identification scheme shown in Fig. 10 and the adopted PWM technique have been implemented on a dSPACE card (DS1103). The sampling time of the identification scheme has been set equal to 10 kHz. The *SynRM* motor is mechanically coupled to a torque controlled *PMSM* drive working as the active load (not necessary in this case). Fig. 11 shows the photo of the *SynRM* drive test set-up.

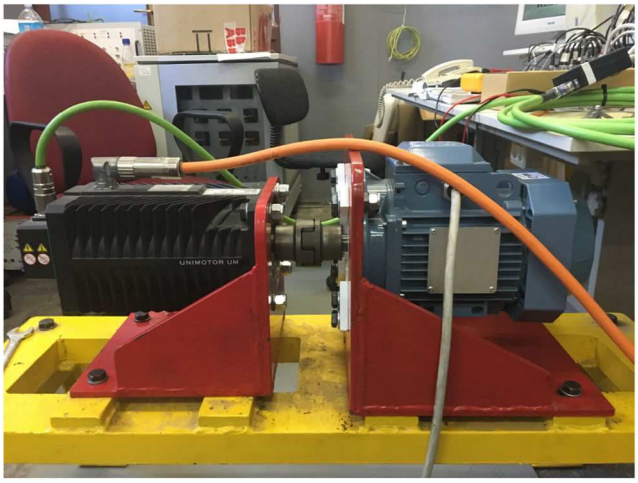

Fig. 11 *Photograph of the experimental set-up with the SynRM*

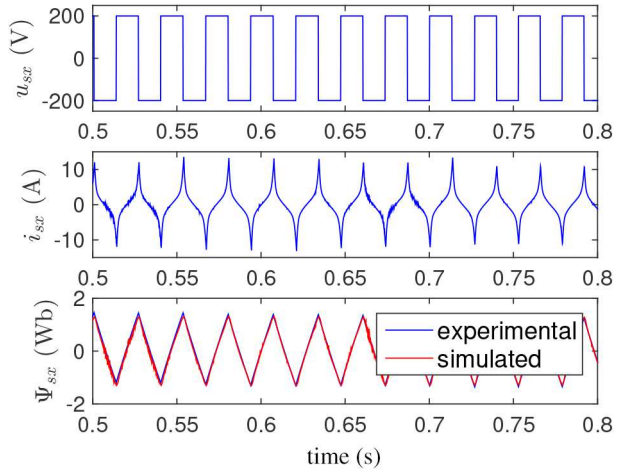

Fig. 12 *u_{sx}, i_{sx}, ψ_{sx} waveforms during the test 1, proposed model*

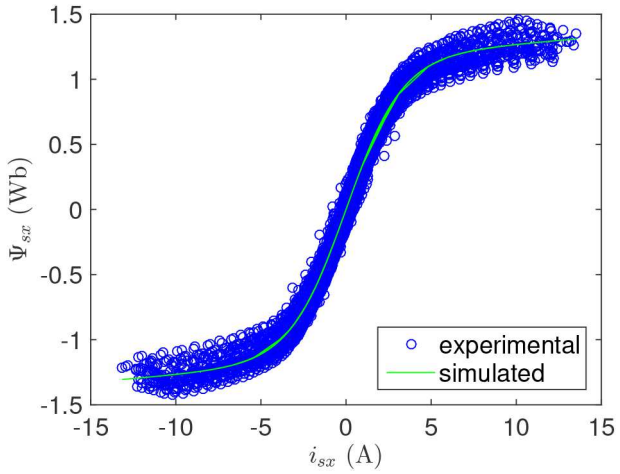

Fig. 13 *$\psi_{sx} = f_1(i_{sx})$ identified at the end of the test 1, proposed model*

6 Experimental results

The parameter estimation technique described in Section 4 has been applied to identify the parameters of the proposed magnetic model described in Section 3.1.

As for the parameter estimation procedure of the *SynRM*, the values of the constant voltage applied to the motor have been selected equal to ±200 and ±100 V, respectively, on the x and y axes, considering that the stator inductance on the y-axis is much lower than that on the x-axis. The limit value of the stator current has been chosen equal to 10 A on the x-axis and 8 A on the y-axis. The current limits have been chosen slightly higher than the rated

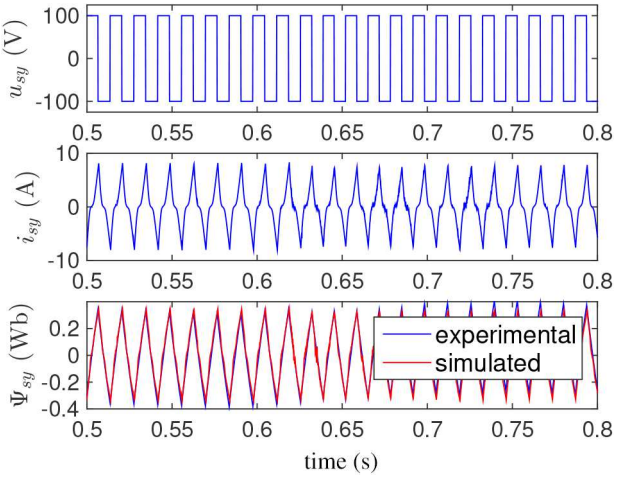

Fig. 14 *u_{sy}, i_{sy}, ψ_{sy} waveforms during the test 2, proposed model*

current of the machine and in any case, big enough to ensure the machine to get full saturation on both axes.

Figs. (12)–(16) describe the experimental results. Fig. 12 is related to test 1 and shows the direct components of the stator voltage, the stator current and the stator flux versus time. In particular, both the measured stator current and the corresponding one computed by the model in (9) are plotted together; the same consideration is valid for the stator flux, which is estimated exploiting (1). As recalled above, the measured flux is itself an estimated quantity. Specifically, the stator flux has been estimated adopting the so-called 'voltage flux model' based on the stator voltage equations. The open-loop integration problem has been solved here adopting the so-called neural adaptive integrator [29].

A good match between the two graphs can be noticed, confirming the validity of the proposed dynamic model as well as its correct parameterisation obtained thanks to the proposed identification technique. The good accuracy in the estimation of the stator currents is confirmed by an equally correct estimation of the stator flux. As a result, Fig. 13 shows the map of the experimental points describing the relationship between the direct component of the stator current and the related stator flux component, as well as the function $\psi_{sx} = f_1(i_{sx})$ computed by the saturation model in (5) on the basis of the measured stator current. Since the x-axis is related to the magnetic circuit with minimum reluctance, the typical effect of the saturation is clearly visible. As for the experimental points, the scattering is caused by two reasons. The first one, is the presence of a certain amount of undesired noise superimposed to the data. Such an effect is limited. The second and more significant one, is the effect of the hysteresis. As a matter of fact, the supply square voltage waveform causes the current to span between high positive and high negative values, with the description of the consequent hysteresis cycle. Such an effect is not considered by the mathematical functions represented by (5), which describe only the saturation phenomenon. The obtained final values of the parameters α_1, β_1, η_1 are shown in Table 2, which shows also the respective mean square errors. Figs. 14 and 15 show the corresponding waveforms related to test 2, which completely characterise the magnetic circuit of the machine on the y-axis.

Since the y-axis is related to the magnetic circuit with maximum reluctance due to the flux barriers, the typical effect of the saturation is less visible and consequently, the $\psi_{sy} = f_2(i_{sy})$ function presents a more linear shape. The obtained final values of the parameters α_2, β_2, η_2 are shown in Table 2. Fig. 16 shows the corresponding time waveforms related to test 3, permitting the characterisation of the cross-saturation effect. It can be seen that the square waveforms of the stator voltages applied to the two axes present frequencies which are multiple of each other, permitting the retrieval of the entire map between the stator flux and currents components. The final values of the parameters γ, μ_1, μ_2, σ_1, σ_2 obtained with this identification process are shown in Table 2.

Fig.s 17 and 18 show the $\psi_{sx} = f_1(i_{sx}, i_{sy})$ and $\psi_{sy} = f_2(i_{sx}, i_{sy})$ surfaces computed with the model in (5), on the basis of the final

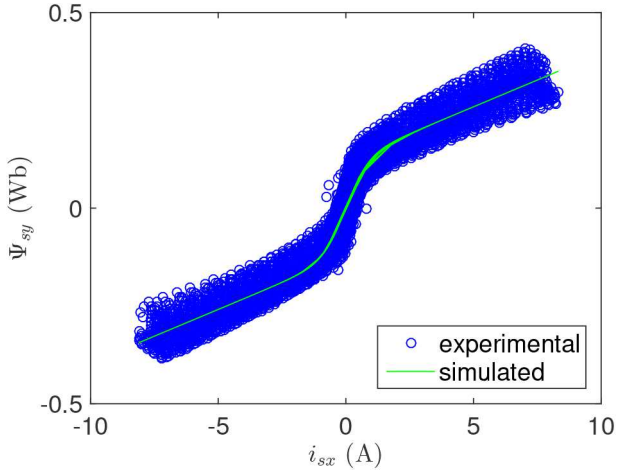

Fig. 15 $\psi_{sy} = f_2(i_{sy})$ *identified at the end of the test 2, proposed model*

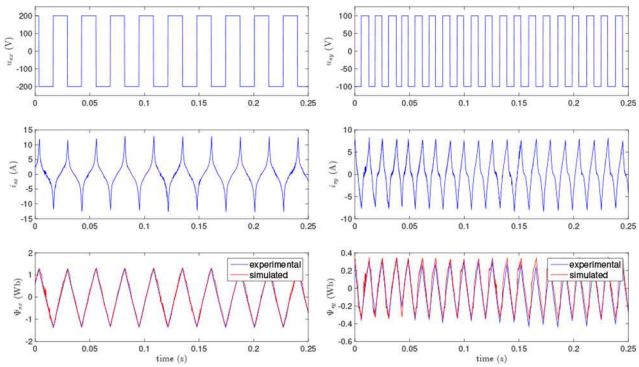

Fig. 16 $u_{sx,y}$, $i_{sx,y}$, $\psi_{sx,y}$ *waveforms during the test 3, proposed model*

Table 2 Identified models parameters

Proposed model		Model in [22]		Model in [23]	
Parameter	Value	Parameter	Value	Parameter	Value
γ	0.1072	L_{0d}	0.239	a_{d0}	5.82
μ_1	3.210	L_{1d}	0.048	a_{dd}	0.823
μ_2	1.4380	β_d	0.005	a_{q0}	29.7
σ_1	0.6987	$I_{th,d}$	3.22	a_{qq}	44.1
σ_2	0.8023	L_{0q}	0.110	a_{dq}	18.8
α_1	1.1627	L_{1q}	0.021	S	6
β_1	0.3044	β_q	0.005	T	1
η_1	$1.0923 \cdot 10^{-2}$	$I_{th,q}$	1.02	U	1
α_2	0.1224			V	0
β_2	1.1125				
η_2	$2.7329 \cdot 10^{-2}$				

values of its identified parameters. These figures also show superimposed the experimental points describing the mapping between the same variables. It can be observed that both computed surfaces properly interpolate the experimental points in the three-dimensional space, confirming the goodness of the proposed saturation model as well as its correct parameterisation.

6.1 Comparison with the magnetic models [22, 23]

In order to highlight the advantages offered by the proposed model in terms of accuracy in approximating the experimental measurements, the parameter estimation technique described in Section 4 has been employed to estimate the parameters of the magnetic models presented in [22, 23]. The finals values of the parameters of the models in [22, 23] are provided in Table 2. With this specific regard, it should be noted that model [22], based on a flux versus current approach, includes only the self-saturation

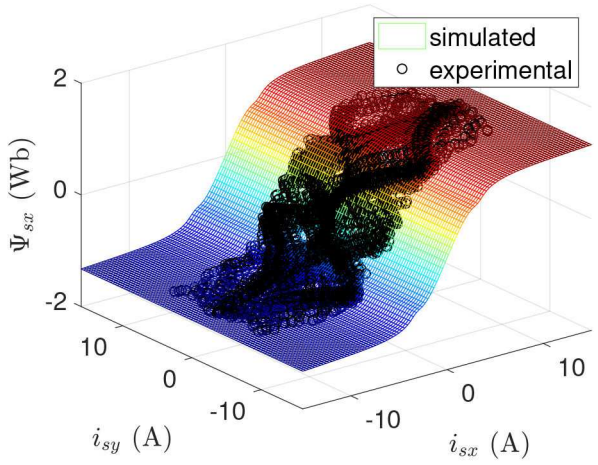

Fig. 17 $\psi_{sx} = f_1(i_{sx}, i_{sy})$ *identified at the end of the test 3, proposed model*

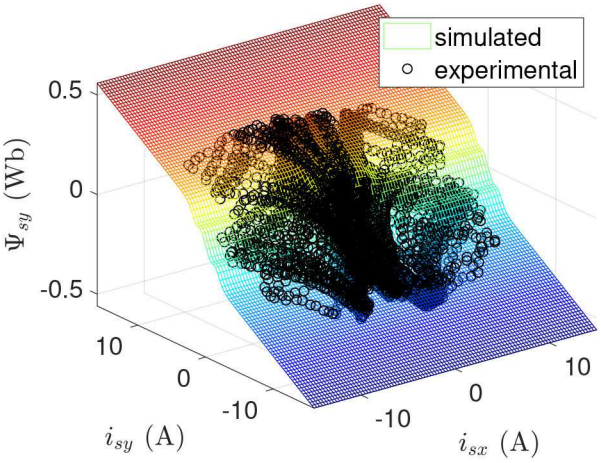

Fig. 18 $\psi_{sy} = f_2(i_{sx}, i_{sy})$ *identified at the end of the test 3, proposed model*

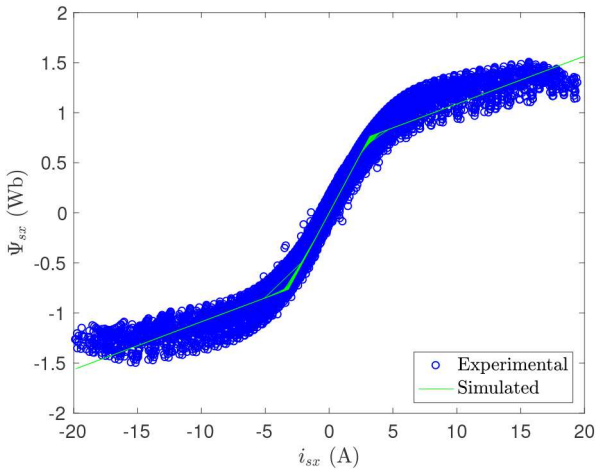

Fig. 19 $\psi_{sx} = h_1(i_{sx})$ *identified at the end of the test 1, model in [22]*

effect, while model [23], based on a current versus flux approach, includes both self- and cross-saturation effects.

Figs. 19 and 20 show the maps of the experimental points describing the relationship between the direct and quadrature components of the stator current and the related stator flux components, as well as the functions $\psi_{sx} = h_1(i_{sx})$, $\psi_{sy} = h_2(i_{sy})$ computed by the self-saturation model in [22], on the basis of the measured stator current. It can be noted that the model in [22] is composed of two branches of linear functions, each characterised by a different rate of change. Remark that, while the $\psi_{sy} = h_2(i_{sy})$ curve quite well interpolates the experimental measurements, because of the more linear nature of the magnetic circuit on the quadrature axis due to the presence of the flux barriers, $\psi_{sx} = h_1(i_{sx})$

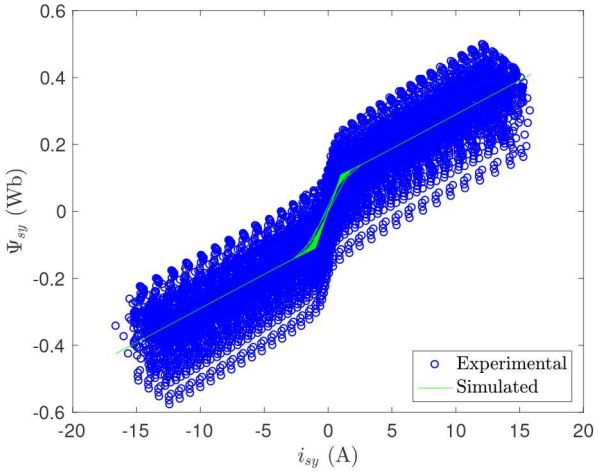

Fig. 20 $\psi_{sy} = h_2(i_{sy})$ *identified at the end of the test 2, model in [22]*

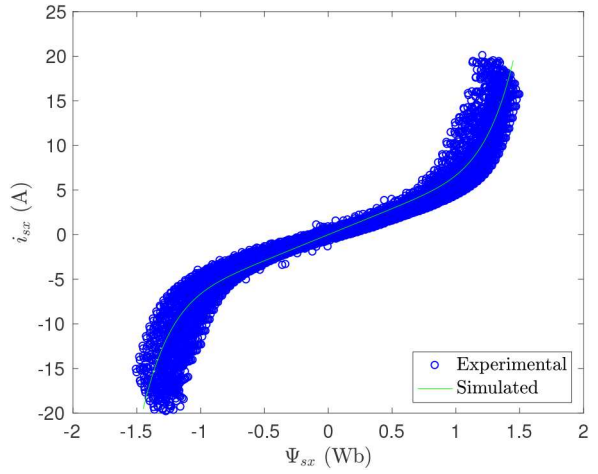

Fig. 21 $i_{sx} = g_1(\psi_{sx})$ *identified at the end of the test 1, model in [23]*

interpolates the experimental measurements with less accuracy, particularly in correspondence of the knee of the saturation curve. Moreover, it is observable that the model fails on the direct axis in a deep saturation region.

Figs. 21 and 22 show the maps of the experimental points describing the relationship between the direct and quadrature components of the stator flux and the related stator current components, as well as the functions $i_{sx} = g_1(\psi_{sx})$, $i_{sy} = g_2(\psi_{sy})$ computed by the self-saturation model in [23], on the basis of the measured flux. It can be noted that the magnetic model in [23] quite well interpolates the experimental points, on both the direct and quadrature axes. As for the curve on the direct axis, the rate of change of the interpolating function does not properly match the one of the experimental points in the linear region, since the slope is slightly higher. Moreover, in the deep saturation region, the interpolating function does not saturate as the experimental points, because of the polynomial nature of the interpolating function. On the contrary, Figs. 13 and 15, related to the proposed magnetic model, show clearly that the proposed model correctly interpolates the experimental points in the entire working region, both in linear zone and in deep saturation.

To confirm what commented above, Table 3 shows a summary of the comparative analysis, in terms of accuracy of estimation, between the proposed model and those presented in [22, 23]. The metric adopted for comparing the accuracies is composed of two indexes: the first is the cost function minimised by GAs (14 and 15), that is linked to the integral of the squared error between the estimated and measured fluxes, the second is the maximum estimation error between the fluxes. It can be observed that the proposed model overcomes those presented in [22, 23], in both the cost function and maximum estimation error. In particular, the maximum estimation errors offered by the models [22, 23] are

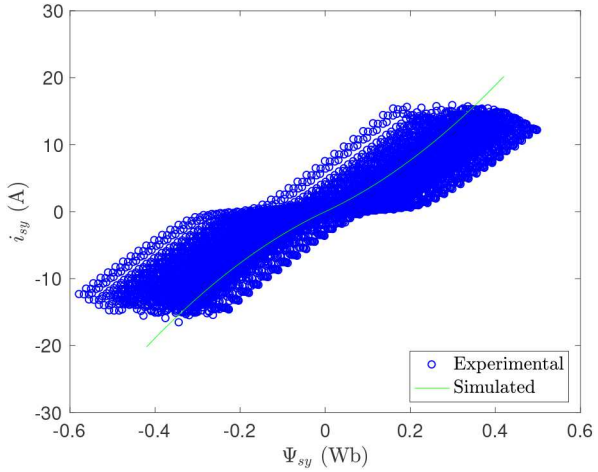

Fig. 22 $i_{sy} = g_2(\psi_{sy})$ *identified at the end of the test 2, model in [23]*

Table 3 Values of the cost functions S_1, S_2 and S_3 (× 100) and maximum estimation error obtained during tests 1, 2 and 3

	Test 1		Test 2		Test 3	
	S_1	e_{max}	S_2	e_{max}	S_3	e_{max}
proposed model	1.7	0.18	1.1	0.11	2.32	1.47
model in [22]	3.02	0.31	1.18	0.25	n.a.	n.a.
model in [23]	2.02	0.3	1.36	0.23	2.86	1.82

much higher than those of the proposed model, on both the direct and quadrature axes. On the direct axis, the percent reduction of the cost function obtained with the proposed model is almost 43% with respect to the model in [22], and 15% with respect to the model in [23]. On the quadrature axis, the percent reduction of the cost function obtained with the proposed model is almost 19% with respect to the model in [22], and 7% with respect to the model in [23]. The increase of overall accuracy achievable with the proposed model is therefore much higher on the direct axis than on the quadrature one, that is to be expected given the higher non-linearity of the magnetic circuit on the direct axis. From this point of view, the model [22] is more accurate than that in [23] on the quadrature axis, which is also to be expected given the higher linearity of the magnetic circuit on the quadrature axis. All the above considerations are confirmed by the maximum estimation error, which is always much lower with the proposed model than with those in [22, 23].

A specific comment should be made on the computational demand of the above three magnetic models. With regard to the computational time, using a laptop with an i5 Intel processor and a 8 Gb DDR3 RAM, the time necessary, for each iteration, is about 15 s both for step 1 and for step 2, and about 20 s for step 3. Moreover, the computational effort for the off-line identification procedure obtained with the proposed model is almost the same as that obtained for the models proposed in [22, 23] with negligible differences.

7 Conclusions

This paper proposes a space-vector dynamic model of the *SynRM* including both self-saturation and cross-saturation effects and selecting as state variables the stator currents. The proposed dynamic model is based on an original function between the stator flux and current components, and relies on 11 coefficients. Starting from the definition of a suitable co-energy function, new flux versus current analytical expression have been retrieved, based on hyperbolic functions. Consequently, the static and dynamic inductances analytical expressions have been deduced as well. Furthermore, the space-vector formulation of the dynamic model adopting the stator currents as state variables has been formulated in both the rotor and stator reference frames. This paper presents also a technique for the estimation of the parameters of the proposed magnetic model, which is based on stand-still tests

without the need of locking the rotor. The identification process is based on the minimisation of a suitably defined error function which includes the difference between the measured and estimated stator fluxes. The proposed parameter estimation technique has been tested in both numerical simulation and experimentally on a suitably developed test set-up. The accuracy of the proposed model has been experimentally compared with other models in the scientific literature, and a precise metric for evaluating the achieved improvements has been adopted.

8 References

[1] Faucher, J., Lajoie-Mazenc, M., Chayegani, A.: 'Characterization of a closed-loop controlled current-fed reluctance machine taking into account saturation', *IEEE Trans. Ind. Appl.*, 1979, **IA-15**, (5), pp. 482–488

[2] Fratta, A., Vagati, A.: 'A reluctance motor drive for high dynamic performance application', *IEEE Trans. Ind. Appl.*, 1992, **28**, (4), pp. 873–879

[3] Matsuo, T., Lipo, T.A.: 'Field oriented control of synchronous reluctance machine'. Proc. of IEEE Power Electronics Specialist Conf. - PESC '93, Seattle, WA, USA, 1993, pp. 425–431

[4] Vagati, A., Pastorelli, M., Scapino, F., *et al.*: 'Impact of cross saturation in synchronous reluctance motors of the transverse-laminated type', *IEEE Trans. Ind. Appl.*, 2000, **36**, (4), pp. 1039–1046

[5] Li, Y., Zhu, Z.Q., Howe, D., *et al.*: 'Modeling of cross-coupling magnetic saturation in signal-injection-based sensorless control of permanent-magnet brushless ac motors', *IEEE Trans. Magn.*, 2007, **43**, (6), pp. 2552–2554

[6] Kuehl, S., Kennel, R.M.: 'Measuring magnetic characteristics of synchronous machines by applying position estimation techniques', *IEEE Trans. Ind. Appl.*, 2014, **50**, (6), pp. 3816–3824

[7] Ibrahim, M.N., Sergeant, P., Rashad, E.M.: 'Relevance of including saturation and position dependence in the inductances for accurate dynamic modeling and control of synrms', *IEEE Trans. Ind. Appl.*, 2017, **53**, (1), pp. 151–160

[8] Yamamoto, S., Hirahara, H., Adawey, J.B., *et al.*: 'Maximum efficiency drives of synchronous reluctance motors by a novel loss minimization controller with inductance estimator', *IEEE Trans. Ind. Appl.*, 2013, **49**, (6), pp. 2543–2551

[9] Armando, E., Guglielmi, P., Pellegrino, G., *et al.*: 'Accurate modeling and performance analysis of ipm-pmasr motors', *IEEE Trans. Ind. Appl.*, 2009, **45**, (1), pp. 123–130

[10] Santos, J.A., Andrade, D.A., Viajante, G.P., *et al.*: 'Analysis and mathematical modeling of the synchronous reluctance motor', *IEEE Latin Am. Trans.*, 2015, **13**, (12), pp. 3820–3825

[11] Uezato, K., Senjyu, T., Tomori, Y.: 'Modeling and vector control of synchronous reluctance motors including stator iron loss', *IEEE Trans. Ind. Appl.*, 1994, **30**, (4), pp. 971–976

[12] Xu, L., Xu, X., Lipo, T.A., *et al.*: 'Vector control of a synchronous reluctance motor including saturation and iron loss', *IEEE Trans. Ind. Appl.*, 1991, **27**, (5), pp. 977–985

[13] Qu, Z., Tuovinen, T., Hinkkanen, M.: 'Inclusion of magnetic saturation in dynamic models of synchronous reluctance motors'. 2012 XXth Int. Conf. on Electrical Machines, Marseille, France, 2012, pp. 994–1000

[14] Mademlis, C.: 'Compensation of magnetic saturation in maximum torque to current vector controlled synchronous reluctance motor drives', *IEEE Trans. Energy Convers.*, 2003, **18**, (3), pp. 379–385

[15] Tuovinen, T., Hinkkanen, M., Luomi, J.: 'Analysis and design of a position observer with resistance adaptation for synchronous reluctance motor drives', *IEEE Trans. Ind. Appl.*, 2013, **49**, (1), pp. 66–73

[16] Kilthau, A., Pacas, J.M.: 'Appropriate models for the control of the synchronous reluctance machine'. Conf. Record of the 2002 IEEE Industry Applications Conf. 37th IAS Annual Meeting (Cat. No.02CH37344), Pittsburgh, PA, USA, 2002, vol. 4, 2289–2295

[17] Corzine, K.A., Kuhn, B.T., Sudhoff, S.D., *et al.*: 'An improved method for incorporating magnetic saturation in the q-d synchronous machine model', *IEEE Trans. Energy Convers.*, 1998, **13**, (3), pp. 270–275

[18] De-Jong, H.: 'Saturation in electrical machines'. Proc. ICEM, Athens, Greece, 1980, vol. 80, 1545–1552

[19] Armando, E., Bojoi, R.I., Guglielmi, P., *et al.*: 'Experimental identification of the magnetic model of synchronous machines', *IEEE Trans. Ind. Appl.*, 2013, **49**, (5), pp. 2116–2125

[20] Pellegrino, G., Boazzo, B., Jahns, T.M.: 'Magnetic model self-identification for pm synchronous machine drives', *IEEE Trans. Ind. Appl.*, 2015, **51**, (3), pp. 2246–2254

[21] Odhano, S.A., Giangrande, P., Bojoi, R.I., *et al.*: 'Self-commissioning of interior permanent- magnet synchronous motor drives with high-frequency current injection', *IEEE Trans. Ind. Appl.*, 2014, **50**, (5), pp. 3295–3303

[22] Bedetti, N., Calligaro, S., Petrella, R.: 'Stand-still self-identification of flux characteristics for synchronous reluctance machines using novel saturation approximating function and multiple linear regression', *IEEE Trans. Ind. Appl.*, 2016, **52**, (4), pp. 3083–3092

[23] Hinkkanen, M., Pescetto, P., Mölsä, E., *et al.*: 'Sensorless self-commissioning of synchronous reluctance motors at standstill without rotor locking', *IEEE Trans. Ind. Appl.*, 2017, **53**, (3), pp. 2120–2129

[24] Accetta, A., Cirrincione, M., Pucci, M., *et al.*: 'A saturation model of the synchronous reluctance motor and its identification by genetic algorithms'. 2018 IEEE Energy Conversion Congress and Exposition (ECCE), 2018, pp. 4460–4465

[25] Accetta, A., Cirrincione, M., Pucci, M., *et al.*: 'A space-vector state dynamic model of the synchronous reluctance motor including self and cross-saturation effects and its parameters estimation'. 2018 IEEE Energy Conversion Congress and Exposition (ECCE), Portland, OR, USA, 2018, pp. 4466–4472

[26] Guglielmi, P., Pastorelli, M., Vagati, A.: 'Impact of cross-saturation in sensorless control of transverse-laminated synchronous reluctance motors', *IEEE Trans. Ind. Electron.*, 2006, **53**, (2), pp. 429–439

[27] Mingardi, D., Morandin, M., Bolognani, S., *et al.*: 'On the proprieties of the differential cross-saturation inductance in synchronous machines', *IEEE Trans. Ind. Appl.*, 2017, **53**, (2), pp. 991–1000

[28] Cheng, R.: '*Genetic algorithms and engineering optimization*' (Wiley-Interscience, USA, 2000)

[29] Cirrincione, M., Pucci, M., Vitale, G.: '*Power converters and AC electrical drives with linear neural networks*', in Emadi, A. (Ed.): *Energy, power electronics and machines*' (Taylor & Francis Group, USA, 2012), pp. 319–374